





## Influence of the Turing instability on the motion of domain boundaries

Isha Gupta <sup>1,\*</sup>, J. R. Barber <sup>1</sup>, M. D. Thouless <sup>1,2</sup> and Wei Lu <sup>1,2</sup>

<sup>1</sup>*Department of Mechanical Engineering, University of Michigan, Ann Arbor, Michigan 48109, USA*

<sup>2</sup>*Department of Materials Science and Engineering, University of Michigan, Ann Arbor, Michigan 48109, USA*



(Received 6 April 2020; accepted 24 June 2020; published 15 July 2020)

Turing's theory of pattern formation has provided crucial insights into the behavior of various biological, geographical, and chemical systems over the last few decades. Existing studies have focused on moving-boundary Turing systems for which the motion of the boundary is prescribed by an external agent. In this paper, we present an extension of this theory to a class of systems in which the front motion is governed by the physical processes that occur within the domain. Biological systems exhibiting apically dominant growth and corrosion of metals and alloys highlight some of the noteworthy examples of such systems. In this study, we characterize the nature of interaction between the moving front and the Turing-instability for both an activator-inhibitor and an activator-substrate model. Behavioral regimes of periodic, as well as nonperiodic (nonconstant), growth rates are obtained. Furthermore, the trends in the first show striking similarities with the cyclic-boundary-kinetics observed in experimental systems. In general, a stationary, periodic structure is also left behind the moving front. If the periodicity of the boundary kinetics agrees with the allowed range of the stable-periodic solutions, the pattern formed tends to persist. Otherwise, it evolves to a nearby energy-minimum either by peak-splitting, peak-decay, or by settling down to a spatially homogeneous state.

DOI: [10.1103/PhysRevE.102.012802](https://doi.org/10.1103/PhysRevE.102.012802)

### I. INTRODUCTION

Alan Turing proposed his pioneering theory for pattern formation in biological systems in 1952 [1]. It relied on the existence of a system of biochemical species he called morphogens (in view of their possible role in determining the structure of living organisms), reacting and diffusing within a tissue. He suggested that the development of patterns in an initially homogeneous embryo (e.g., leaves arranging periodically on a plant stem) can correspond to the stable stationary waves of the concentration of morphogens generated as the result of an instability of the homogeneous equilibrium state. The simplicity of the theory, and its capability to produce a wide range of distinctive patterns, has triggered significant efforts to find specific applications. Murray's [2] extension of this work, in a paper titled "How the Leopard Gets Its Spots", shows striking similarities between simulated Turing patterns and the stripes or spots observed on various mammalian coats. Kondo *et al.* [3] used this framework to simulate stripes on the marine angelfish, *Pomacanthus*, showing that it can explain the observation that the stripe spacing remains constant as the fish grows. Meinhardt *et al.* [4] proposed a reaction-diffusion model that accurately reproduced the diverse patterns observed on the shells of mollusks. A recent study [5] indicated that the skin denticles on sharks, the structures that allow them to swim swiftly, could also be a result of an underlying Turing mechanism. Though originally developed and applied extensively to the field of developmental biology, as discussed above [2–7], the mathematical formalism of the theory has also been found to be applicable to a much broader range

of scientific problems, including the study of geological and demographic patterns [8,9].

#### A. Mathematical structure

A Turing system is typically characterized by the evolution of spatial patterns in the concentrations or values  $u(x, t)$ ,  $v(x, t)$  of two interacting species, where  $x$  and  $t$  correspond to spatial and temporal coordinates, respectively. Such a system with linear diffusion can be described by the differential equations

$$\begin{aligned}\frac{\partial u}{\partial t} &= D_u \frac{\partial^2 u}{\partial x^2} + f(u, v), \\ \frac{\partial v}{\partial t} &= D_v \frac{\partial^2 v}{\partial x^2} + g(u, v),\end{aligned}\quad (1)$$

where  $D_u$  and  $D_v$  are the diffusion coefficients for  $u$  and  $v$ , respectively. The functions  $f(u, v)$  and  $g(u, v)$  define the influence of each concentration on its own growth rate, and also the coupling between the two concentrations. Instabilities can occur, leading to pattern formation, if one species (the *activator*) has a promoting effect on itself, while the other suppresses itself. Here we shall take  $v$  to represent the activator, in which case the inequalities

$$\begin{aligned}\frac{\partial g(u, v)}{\partial v} &> 0, \quad \frac{\partial f(u, v)}{\partial u} < 0, \\ \frac{\partial g(u, v)}{\partial u} \frac{\partial f(u, v)}{\partial v} &< 0, \quad D_u > D_v\end{aligned}\quad (2)$$

define a necessary but not sufficient condition for pattern formation. The inequality  $D_u > D_v$  requires that the activator should be less mobile than  $u$ .

The third inequality in Eq. (2) implies that  $u$  and  $v$  have opposite effects on each other and can be satisfied in two

\*ishag@umich.edu

different ways, i.e.,

$$\frac{\partial g(u, v)}{\partial u} < 0 \quad \text{and} \quad \frac{\partial f(u, v)}{\partial v} > 0, \quad (3)$$

or

$$\frac{\partial g(u, v)}{\partial u} > 0 \quad \text{and} \quad \frac{\partial f(u, v)}{\partial v} < 0. \quad (4)$$

The conditions (3) define an *activator-inhibitor system* since  $v$  activates both itself and  $u$ , while the *inhibitor*  $u$  suppresses both itself and  $v$ . By contrast, Eq. (4) defines an *activator-substrate system*, in which  $u$  suppresses itself but promotes  $v$ , while  $v$  promotes itself and suppresses  $u$ . In this case  $u$  is called the *substrate* since it is consumed while producing the activator  $v$ .

### B. Moving boundary problems

Several forms were proposed for the interaction functions  $f(u, v)$ ,  $g(u, v)$ , and were shown to be capable of predicting the development of Turing patterns in appropriate parameter ranges [10–12]. Many of these studies focused on fixed spatial domains, but the results proved useful in interpreting the experimentally observed behavior of physical systems where the domain grows in time [5,13]. Crampin *et al.* [14] developed a rigorous analytical framework for problems of this class, and demonstrated the significance of domain growth as a possible mechanism for reliability in pattern selection. In particular, the long-time pattern is then independent of the initial conditions, in contrast to results for fixed domains [14,15]. This framework has been applied to systems where all elements of the spatial domain grow either at a prescribed growth rate [14–17] or at a rate that is controlled by the species or reactants [18,19]. Recently, the analysis of such systems was extended to include the effect of anisotropy in growth rates and the curvature of growing ellipsoidal surfaces [20]. This case of bulk growth is appropriate for a wide variety of biological systems, where each tissue within the domain grows in size. However, there is another class of spatially patterned systems where the domain grows only locally, at a domain boundary or interface (for example, apically growing biological systems [21], oxide layers formed on certain alloys [22], and cloud patterns [23]).

Crampin *et al.* [16] simulated Turing systems with a moving domain boundary and observed the development of a stationary periodic structure behind the moving front. Similar results were obtained by other authors [24–26], but all these investigations were restricted to systems in which the boundary was prescribed to move at a constant rate. However, we are interested in physical systems for which the boundary or interface motion is not prescribed by an external agent, but results from the physics within the domain, such as local concentrations of species. For example, pollen tubes, which exhibit localized growth at a tip [27], are observed to have oscillatory growth rates [28] and periodic depositions of certain pectins [29]. In oxide films formed on zirconium alloys, periodic increases from an approximately parabolic rate of the metal-oxide interface movement (which, like many other oxidation processes [30], is controlled by the local concentration of the oxygen ions) are observed [22]. Additionally, the oxide film exhibits a layered structure that is directly correlated with

this periodicity [22]. To the best of our knowledge, there are no existing theories which provide a rigorous explanation of the phenomena discussed above.

In this paper, we investigate the interaction between a pattern-causing Turing instability and the motion of a domain boundary for cases where the instantaneous boundary velocity is driven by a local concentration. In particular, we shall document the nature of this interaction in the context of Gierer-Meinhardt's activator-inhibitor model, and Schnakenberg's activator-substrate model, as shown in the next section.

## II. ACTIVATOR-INHIBITOR SYSTEM

Gierer-Meinhardt's activator-inhibitor model can be expressed in dimensionless form as

$$\begin{aligned} \frac{\partial \tilde{u}}{\partial \tilde{t}} &= \frac{\partial^2 \tilde{u}}{\partial \tilde{x}^2} - \tilde{u} + \tilde{v}^2, \\ \frac{\partial \tilde{v}}{\partial \tilde{t}} &= R_D \frac{\partial^2 \tilde{v}}{\partial \tilde{x}^2} + \tilde{c}_3 \frac{\tilde{v}^2}{\tilde{u}} - \tilde{c}_4 \tilde{v} \end{aligned} \quad (5)$$

(see Appendix A), where  $R_D = D_v/D_u$ ,  $\tilde{c}_3$ ,  $\tilde{c}_4$  are dimensionless constants and  $\tilde{u}$ ,  $\tilde{v}$ ,  $\tilde{x}$  and  $\tilde{t}$  are dimensionless versions of the parameters and coordinates introduced in Eq. (1). These equations have a homogeneous steady-state solution

$$\tilde{v} = \frac{\tilde{c}_3}{\tilde{c}_4}, \quad \tilde{u} = \left( \frac{\tilde{c}_3}{\tilde{c}_4} \right)^2 \quad (6)$$

in an infinite spatial domain, but this is unstable in the range

$$\frac{\tilde{c}_4}{R_D} > \frac{1}{(3 - 2\sqrt{2})} \approx 5.82, \quad (7)$$

(see Appendix A). This instability results in the formation of the stationary, periodic concentration profiles in an infinite spatial domain, associated with Turing patterns [10]. In a finite fixed domain, the periodicity may be modified near the boundaries to adjust to the boundary conditions.

In this paper, we consider the domain defined by  $0 < \tilde{x} < \tilde{h}(\tilde{t})$ , where  $\tilde{x} = 0$  is a fixed boundary, and  $\tilde{x} = \tilde{h}(\tilde{t})$  is a moving boundary whose motion is determined by local concentrations. In particular, we assume

$$\frac{d\tilde{h}}{d\tilde{t}} = \tilde{k}\tilde{u}(\tilde{h}, \tilde{t}), \quad (8)$$

where  $\tilde{k}$  is a constant that might represent a reaction constant if the boundary motion is associated with a chemical reaction [30]. At the fixed boundary  $\tilde{x} = 0$ , we assume

$$\tilde{u}(0, \tilde{t}) = \tilde{u}_0 \quad \text{and} \quad \frac{\partial \tilde{v}}{\partial \tilde{x}}(0, \tilde{t}) = 0, \quad (9)$$

and at the moving boundary,

$$\tilde{v}(\tilde{h}, \tilde{t}) = \tilde{v}_{\tilde{h}} \quad \text{and} \quad -\frac{\partial \tilde{u}}{\partial \tilde{x}}(\tilde{h}, \tilde{t}) = [\tilde{u}(\tilde{h}, \tilde{t}) + \tilde{Q}] \frac{d\tilde{h}}{d\tilde{t}}. \quad (10)$$

The last condition represents a flux balance for the species  $\tilde{u}$ , with the constant  $\tilde{Q}$  representing the amount of  $\tilde{u}$  consumed per unit area in moving the boundary through a unit distance. If the species  $\tilde{u}$  acts only as a catalyst for the process that drives the boundary motion,  $\tilde{Q}$  may be taken as zero.

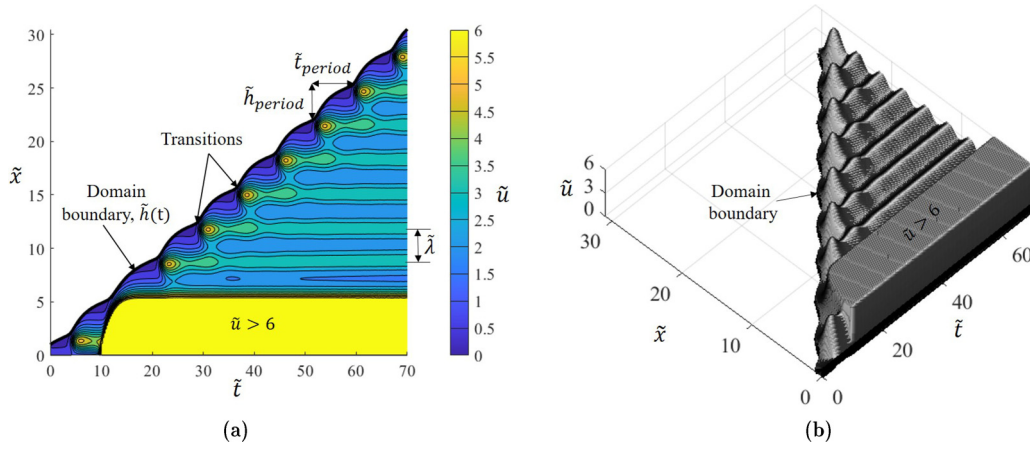


FIG. 1. Periodic behavior: (a) Contours of  $\tilde{u}$  showing periodic transitions between convex-upward segments of the boundary kinetics, each caused by a peak in  $\tilde{u}$  at the moving front. The distance traversed between two transitions,  $\tilde{h}_{\text{period}}$ , is equal to the wavelength ( $\tilde{\lambda}$ ) of the stationary pattern left behind the moving front. (b) Spatiotemporal concentration profile for the species  $\tilde{u}$  showing development of peaks at the moving front.  $\tilde{x}$  is the distance from the fixed surface. Results are obtained using Gierer-Meinhardt activator ( $v$ )-inhibitor ( $u$ ) kinetics with  $\tilde{c}_4 = 0.6$ ,  $R_D = 3/40$ ,  $\tilde{c}_3 = 1$ ,  $\tilde{u}_0 = 1$ ,  $\tilde{v}_h = 0.3$ ,  $\tilde{Q} = 1$ , and  $\tilde{k} = 1$ .

### A. Numerical procedure

For the numerical solution of these equations, it is convenient to use the coordinate transformation  $\tilde{x} = \zeta \tilde{h}(\tilde{t})$  to convert the problem to one on the fixed domain  $0 < \zeta < 1$ . The governing equations then take the form

$$\frac{\partial \tilde{u}}{\partial \tilde{t}} = \frac{\zeta}{\tilde{h}} \frac{d\tilde{h}}{d\tilde{t}} \frac{\partial \tilde{u}}{\partial \zeta} + \frac{1}{\tilde{h}^2} \frac{\partial^2 \tilde{u}}{\partial \zeta^2} - \tilde{u} + \tilde{v}^2, \quad (11)$$

$$\frac{\partial \tilde{v}}{\partial \tilde{t}} = \frac{\zeta}{\tilde{h}} \frac{d\tilde{h}}{d\tilde{t}} \frac{\partial \tilde{v}}{\partial \zeta} + \frac{R_D}{\tilde{h}^2} \frac{\partial^2 \tilde{v}}{\partial \zeta^2} + \tilde{c}_3 \frac{\tilde{v}^2}{\tilde{u}} - \tilde{c}_4 \tilde{v}, \quad (12)$$

$$\frac{d\tilde{h}}{d\tilde{t}} = \tilde{k} \tilde{u}(1, \tilde{t}), \quad (13)$$

with boundary conditions

$$\begin{aligned} \tilde{u}(0, \tilde{t}) = \tilde{u}_0, \quad \frac{\partial \tilde{v}}{\partial \zeta}(0, \tilde{t}) = 0, \quad \tilde{v}(1, \tilde{t}) = \tilde{v}_h, \\ -\frac{\partial \tilde{u}}{\partial \zeta}(1, \tilde{t}) = \tilde{h}[\tilde{u}(1, \tilde{t}) + \tilde{Q}] \frac{d\tilde{h}}{d\tilde{t}}. \end{aligned} \quad (14)$$

This system of equations was solved using the finite-element-based software package FLEX-PDE professional version 7.15.

To start the solution procedure, we needed to define a finite initial domain size  $\tilde{h}(0) \equiv \tilde{h}_0$  and the corresponding initial spatial distributions  $\tilde{u}(\zeta, 0)$ ,  $\tilde{v}(\zeta, 0)$ . Here we used  $\tilde{h}_0 = 1$  and simple linear distributions, with parameters chosen to satisfy Eqs. (13) and (14). In general, the numerical results were found to be insensitive to initial conditions once the domain size was large compared with  $\tilde{h}_0$ .

### B. Characterization of the model response

The response of the model can be periodic or nonperiodic depending on the values of the dimensionless parameters  $\tilde{c}_3$ ,  $\tilde{c}_4$ ,  $R_D$ ,  $\tilde{k}$ ,  $\tilde{Q}$  and the boundary values  $\tilde{u}_0$  and  $\tilde{v}_h$ . In this section, we shall give illustrations of several kinds of behavior, and some indication of the parameter ranges in which they are to be expected.

The simplest class of behavior is that where the inequality (7) is not satisfied, so that the homogeneous solution is stable. In this case, the moving boundary may advance at a constant rate, or it may show periodic variations depending on parameter values, but the distributions of  $\tilde{u}$ ,  $\tilde{v}$  eventually converge on the homogeneous solution (6), except in regions adjacent to the instantaneous domain boundaries.

If the homogeneous solution is unstable, the distributions far from the moving front should be unaffected by it, and hence must converge on a steady state that is stable in an infinite domain. In Appendix B, we determine both stable and unstable periodic steady-state solutions of Eq. (5), using the MATLAB package PDE2PATH [31,32]. For given parameter values satisfying Eq. (7), stable periodic solutions exist in a finite range of wavelengths, the upper bound of which is significantly higher than that obtained by linear perturbation of the homogeneous solution. For systems not satisfying Eq. (7), no periodic solutions are obtained.

#### 1. Periodic behavior

Figure 1 shows (a) contours of  $\tilde{u}$  and the motion of the domain boundary  $\tilde{h}(\tilde{t})$ , and (b) the spatiotemporal distributions of  $\tilde{u}$  (following the work of Crampin *et al.* [14]), for the parameter values  $\tilde{c}_3 = 1$ ,  $\tilde{c}_4 = 0.6$ ,  $R_D = 3/40$ ,  $\tilde{k} = 1$ ,  $\tilde{Q} = 1$  and boundary values  $\tilde{u}_0 = 1$ ,  $\tilde{v}_h = 0.3$ . In Fig. 1(a), segments of “convex-upward” boundary kinetics are separated by rapid changes of velocity, which we refer to as “transitions”. Each transition corresponds to the formation of a peak in the concentrations of both  $\tilde{u}$  [as shown in Fig. 1(b)] and  $\tilde{v}$ . After the passage of the moving boundary, the spatial distributions rapidly converge on a stationary periodic pattern (except near the fixed boundary) in which the peaks of  $\tilde{u}$  and  $\tilde{v}$  coincide. In Fig. 1, each transition corresponds to a peak at the moving boundary and these peaks persist so that the resulting stationary pattern has dimensionless wavelength  $\tilde{\lambda}$ , equal to the advance  $\tilde{h}_{\text{period}}$  of the moving front between successive transitions. However, if  $\tilde{c}_4$  is increased to 1.4, keeping the other parameters unchanged, the function  $\tilde{h}(\tilde{t})$  has a periodic

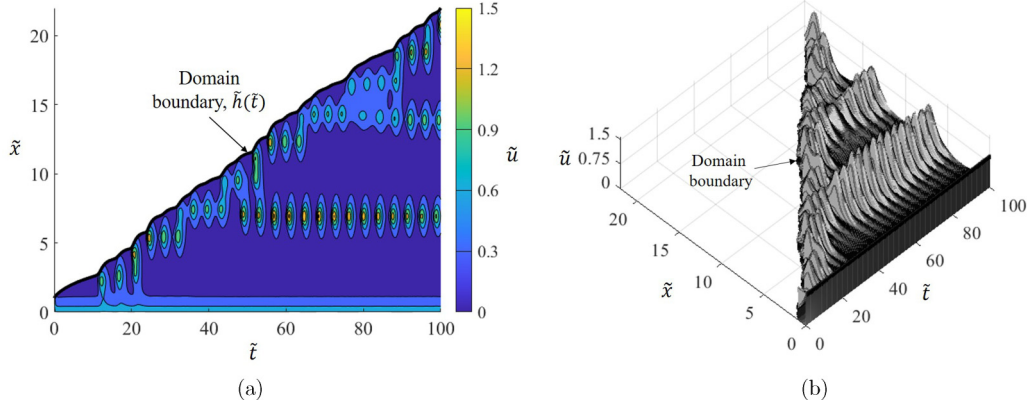


FIG. 2. Random behavior: (a) Contours of  $\tilde{u}$  showing erratic boundary kinetics. (b) Spatiotemporal evolution of the species  $\tilde{u}$  showing random development of peaks at the moving boundary, and the following erratic fluctuations in the amplitude for Gierer-Meinhardt activator ( $v$ )-inhibitor ( $u$ ) kinetics with  $\tilde{c}_4 = 1.8$ ,  $R_D = 3/40$ ,  $\tilde{c}_3 = 1$ ,  $\tilde{u}_0 = 1$ ,  $\tilde{v}_h = 0.3$ ,  $\tilde{Q} = 1$ , and  $\tilde{k} = 1$ . Homogeneous initial conditions consistent with the boundary conditions are used.

form similar to that in Fig. 1(a), but behind the moving front every second peak starts to decay, and the pattern eventually evolves to one with a wavelength  $\tilde{\lambda} = 2\tilde{h}_{\text{period}}$ .

Fixed-domain simulations (see Appendix B) using these parameter values show that steady-state periodic solutions do exist with a wavelength  $\tilde{\lambda} = \tilde{h}_{\text{period}}$ , but they are unstable. Thus, the moving front imposes a certain periodicity on the pattern, but its persistence as a steady state or its subsequent evolution depend on features of the equation system that are independent of the domain size or its evolution in time.

## 2. Random behaviour

If  $\tilde{c}_4$  is increased further to 1.8 while keeping the other parameters unchanged from those used in Fig. 1, the boundary velocity exhibits essentially random perturbations from an otherwise linear trend as shown in Fig. 2(a). The corresponding concentrations of  $\tilde{u}$  at the moving boundary also fluctuate randomly, but as the boundary recedes, the distributions evolve into relatively isolated peaks as shown in Fig. 2(b). The amplitudes of these peaks fluctuate erratically, with some decaying eventually to zero. The others stabilize at a more or less reproducible maximum value, which for these parameter values is  $\tilde{u}_{\text{max}} \approx 0.64$ ,  $\tilde{v}_{\text{max}} \approx 1.56$ . Throughout this transient process, the peaks in  $\tilde{u}$  and  $\tilde{v}$  remain spatially coincident.

## 3. Periodic boundary motion without patterns

If  $\tilde{c}_4$  in the above case is increased beyond about 1.9, the boundary motion reverts to a convex-upward periodic form like that in Fig. 1(a), but the distributions of  $\tilde{u}$  and  $\tilde{v}$  then decay asymptotically to zero, so that regions away from the boundaries eventually become completely devoid of both species. At first sight, this appears to be inconsistent with the presence of the term  $\tilde{c}_3\tilde{v}^2/\tilde{u}$  in Eq. (5). However, if we assume that  $\tilde{u}, \tilde{v}$  are spatially homogeneous and that  $\tilde{v} \ll \tilde{u}$ , these equations can be approximated as

$$\frac{d\tilde{u}}{d\tilde{t}} + \tilde{u} = 0, \quad \frac{d\tilde{v}}{d\tilde{t}} + \tilde{c}_4\tilde{v} = 0, \quad (15)$$

with solution  $\tilde{u} = C \exp(-\tilde{t})$ ,  $\tilde{v} = D \exp(-\tilde{c}_4\tilde{t})$  where  $C, D$  are constants. The condition  $\tilde{v} \ll \tilde{u}$  then reduces to

$$\frac{D}{C} \exp[(1 - \tilde{c}_4)\tilde{t}] \ll 1, \quad (16)$$

which will be satisfied for all  $\tilde{t}$  if  $\tilde{c}_4 > 1$  and the initial conditions are chosen such that  $D/C \ll 1$ . Thus  $\tilde{c}_4 > 1$  is a necessary but not sufficient condition for  $\tilde{u}$  and  $\tilde{v}$  to decay towards zero, as is shown by the results described above for  $\tilde{c}_4 = 1.4$  and 1.8.

## C. Dependence of Turing-pattern wavelength on boundary kinetics

For the Gierer-Meinhardt model, Turing patterns correspond to stable time-invariant periodic solutions of Eq. (5). The results described above show that boundary kinetics have a significant effect on the distributions generated immediately behind the moving front, but the resulting patterns persist only if they lie in the appropriate stable wavelength range (see Appendix B), or if they can evolve to such a wavelength.

Figure 3 shows the wavelength of the resulting steady-state pattern as a function of the growth-rate parameter  $\tilde{k}$  in Eq. (8) for two sets of parameter values, A: [ $R_D = 1/16$ ,  $\tilde{c}_3 = 0.83$ ,  $\tilde{v}_h = 0.3$ ] and B: [ $R_D = 3/40$ ,  $\tilde{c}_3 = 1.0$ ,  $\tilde{v}_h = 0.1$ ]. The remaining parameters  $\tilde{c}_4 = 0.5$ ,  $\tilde{u}_0 = 1$ , and  $\tilde{Q} = 1$  are common to both cases. The dashed lines in Fig. 3 represent the lower ( $\tilde{\lambda}_1$ ) and upper ( $\tilde{\lambda}_2$ ) bounds of the range of wavelengths of stable periodic patterns obtained numerically, as discussed in Appendix B. Notice that the upper bound for case [A] is approximately  $\tilde{\lambda}_2^A \approx 21$  so does not appear in Fig. 3.

Case [A] corresponds to the ratio  $\tilde{c}_4/R_D = 8$ , which is well above the boundary for the instability defined in Eq. (7). At lower values of  $\tilde{k}$ , the wavelength generated at the moving front is retained in the steady state, and it decreases monotonically as  $\tilde{k}$  is increased over five orders of magnitude. However, for  $\tilde{k} > 1$  some of the peaks generated decay, leading to a larger steady-state wavelength, as discussed in Sec. II B 1. These results are indicated by triangles in Fig. 3.

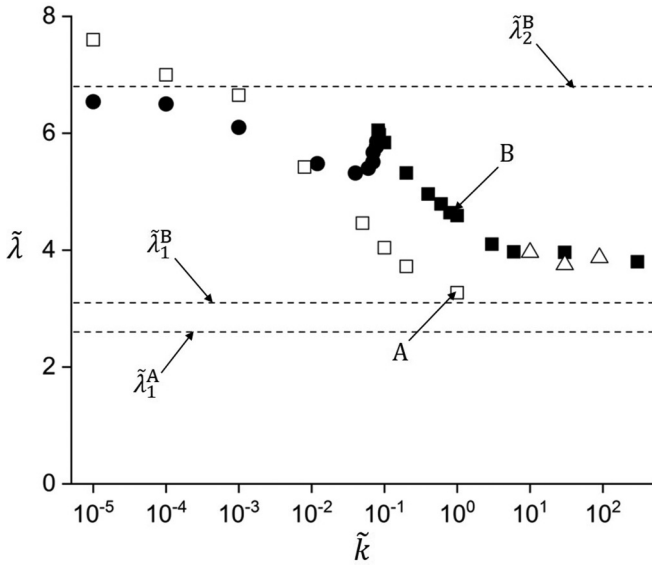


FIG. 3. Turing-pattern wavelength as a function of the growth-rate parameter  $\tilde{k}$  in Eq. (8). Hollow symbols [A] are for  $R_D = 1/16$ ,  $\tilde{c}_3 = 0.83$ ,  $\tilde{v}_h = 0.3$  and solid symbols [B] are for  $R_D = 3/40$ ,  $\tilde{c}_3 = 1.0$ ,  $\tilde{v}_h = 0.1$ . In both cases,  $\tilde{c}_4 = 0.5$ ,  $\tilde{u}_0 = 1$ , and  $\tilde{Q} = 1$ . Triangles identify cases leading to peak decay, while circles identify cases of peak splitting. Dashed lines represent bounds on wavelengths of stable patterns (see Appendix B).

Case [B] corresponds to  $\tilde{c}_4/R_D = 6.7$ , for which a narrower range of wavelengths is stable in the steady state. The actual wavelength increases with decreasing  $\tilde{k}$  down to  $\tilde{k} \approx 0.1$ , below which some of the generated peaks split into two through a transient process that we describe in more detail in Sec. II C 1. Steady-state patterns generated by peak splitting are indicated by circles in Fig. 3. Notice that peak splitting occurs before  $\tilde{h}_{\text{period}}$  reaches values for which steady-state patterns are unstable. To elucidate this behavior, we performed numerical simulations on a large fixed domain with periodic initial conditions of wavelength close to the upper boundary

in Fig. 3. Results show that the pattern converges on the steady state only if the initial distributions are very close to those in the steady state. With all other initial conditions, the system preferentially evolves towards a pattern with a different wavelength.

1. Peak-splitting

In the previous section, we noted that peak splitting causes the wavelength of the final pattern for case [B] to differ from that generated at the moving front as this wavelength approaches the upper boundary of the range of stable Turing patterns for certain parameter values. Figure 4 shows this evolutionary process for  $\tilde{u}(\tilde{x}, \tilde{t})$  with  $\tilde{k} = 1$ . For instance, Fig. 4(a) shows that at  $\tilde{t} \approx 1475$ , a peak develops rapidly near  $\tilde{x} = 41$ . The shape of this peak changes relatively slowly until  $\tilde{t} \approx 1620$ , at which time it starts to split into two peaks. As these new peaks develop, they also move apart. The right peak moves to the right, and eventually stabilizes at  $\tilde{x} \approx 40$ , while the left peak moves a larger distance to the left, reaching the location  $\tilde{x} \approx 47.5$ . Such an event is observed to occur periodically. The corresponding influence on the motion of the boundary is shown in Fig. 4(b). The initial peak development is associated with a large increase in boundary velocity  $\dot{\tilde{h}}$  labeled “strong transition” while the peak-splitting event gives only a minor perturbation in the velocity. Strong transitions are separated by a distance  $2\tilde{\lambda}$ , where  $\tilde{\lambda}$  is the wavelength of the resulting Turing pattern.

The number of peaks that split in case [B] depends on the value of  $\tilde{k}$  and appears to self-select a value that results in a wavelength well within the steady-state bounds. For example, the points shown in Fig. 3 for case [B] as  $\tilde{k}$  is decreased in the range  $0.1 > \tilde{k} > 0.05$  include cases where (i) one out of four, or (ii) two out of every five peaks split, or (iii) each newly generated peak splits four times. In each case, the resulting pattern then adjusts as in Fig. 4 to give a uniform spacing in the steady state.

At even lower values of  $\tilde{k}$ , a single peak is generated at the moving boundary when the process starts; thereafter, all

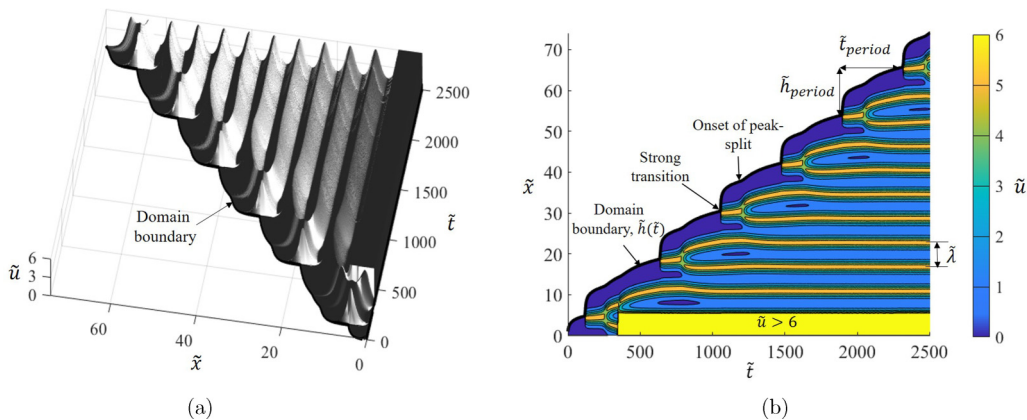


FIG. 4. Periodic behavior with peak-splitting: (a) Spatiotemporal evolution of the species  $\tilde{u}$  showing each peak formed at the boundary splitting once. (b) Contours of  $\tilde{u}$  showing a strong transition in the boundary kinetics for each peak formed at the boundary. The peaks farther away from the moving front are observed to be stationary with a wavelength of  $\tilde{\lambda}$ . Strong transitions are separated by a distance  $\tilde{h}_{\text{period}} = 2\tilde{\lambda}$ . Results are obtained using Gierer-Meinhardt activator ( $v$ )-inhibitor ( $u$ ) kinetics with  $\tilde{c}_4 = 0.5$ ,  $R_D = 3/40$ ,  $\tilde{c}_3 = 1$ ,  $\tilde{u}_0 = 1$ ,  $\tilde{v}_h = 0.01$ ,  $\tilde{Q} = 1$ , and  $\tilde{k} = 1$ .

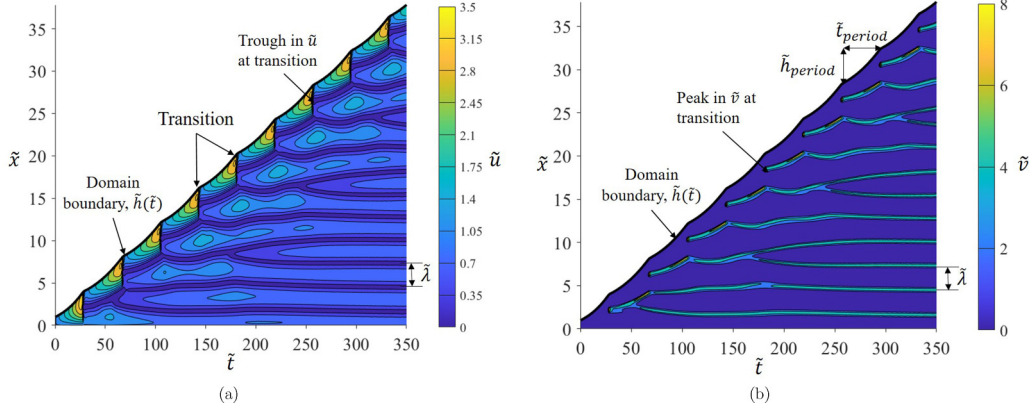


FIG. 5. Behavior of Schnakenberg's activator-substrate model for  $R_D = 3/400$ ,  $\tilde{a} = 0.9$ ,  $\tilde{b} = 0.1$ ,  $\tilde{u}_0 = 1$ ,  $\tilde{v}_h = 0.1$ ,  $\tilde{Q} = 1$ , and  $\tilde{k} = 0.05$ . (a) Contours of  $\tilde{u}$  showing troughs developed at the boundary causing periodic transitions between concave-upward segments, in contrast with the convex-upwards behavior in Fig. 1(b). (b) Contours of  $\tilde{v}$  show every second peak formed at the boundary splitting. The peaks farther away from the moving front are observed to be stationary. Peaks in  $\tilde{v}$  coincide with troughs in  $\tilde{u}$ . Transitions are separated by a distance  $\tilde{h}_{\text{period}} = (3/2)\tilde{\lambda}$ .  $\tilde{x}$  is the distance from the fixed surface.

subsequent peaks are generated by splitting the peak nearest the moving boundary. In this case, there are no strong transitions of the form shown in Fig. 4(b), and the boundary kinetics are only slightly perturbed from linear.

These results are obtained using numerical simulations, and, hence, we can only investigate cases with particular parameter values. However, to give a broader picture of the system behavior, Appendix C presents a map showing the dependence of qualitative features of the behavior as functions of  $\tilde{v}_h$  and  $\tilde{c}_4$ .

### III. ACTIVATOR-SUBSTRATE SYSTEM

We next consider Schnakenberg's activator-substrate model [11], which can be described in the dimensionless form

$$\begin{aligned} \frac{\partial \tilde{u}}{\partial \tilde{t}} &= \frac{\partial^2 \tilde{u}}{\partial \tilde{x}^2} + \tilde{a} - \tilde{v}^2 \tilde{u}, \\ \frac{\partial \tilde{v}}{\partial \tilde{t}} &= R_D \frac{\partial^2 \tilde{v}}{\partial \tilde{x}^2} + \tilde{b} + \tilde{v}^2 \tilde{u} - \tilde{v}, \end{aligned} \quad (17)$$

[see Appendix D], where  $\tilde{u}$ ,  $\tilde{v}$  act as substrate and activator, respectively, and  $R_D \ll 1$ . As in Sec. II, we assume that the velocity of the moving front is determined by Eq. (8), and the remaining boundary conditions by Eqs. (9) and (10).

Figure 5 shows the response of the system for parameter values  $R_D = 3/400$ ,  $\tilde{a} = 0.9$ ,  $\tilde{b} = 0.1$ ,  $\tilde{u}_0 = 1$ ,  $\tilde{v}_h = 0.1$ ,  $\tilde{Q} = 1$ , and  $\tilde{k} = 0.05$ . Troughs in the substrate concentration  $\tilde{u}$  [Fig. 5(a)], and simultaneous peaks in the activator concentration  $\tilde{v}$  [Fig. 5(b)], are developed periodically at the moving boundary. These events are associated with a transient reduction in domain growth rate, leading to the concave-upwards boundary kinetics, in contrast to the convex-upwards kinetics of the Gierer-Meinhardt model in Fig. 1(a).

Figure 5 also shows that for these set of parameters, every second peak generated at the moving boundary splits. Also, the splitting process initiates when this peak is two peaks away from the boundary. The distribution, therefore, eventually converges on a stationary periodic pattern, with  $\tilde{\lambda} = (2/3)\tilde{h}_{\text{period}}$ .

### IV. CONCLUSION

In this paper, we examine the interaction between pattern-forming Turing instabilities and a domain boundary whose motion is governed by the local concentration of one of the species. Results for both the Gierer-Meinhardt activator-inhibitor model [10] and the Schnakenberg activator-substrate model [11] show parameter ranges in which the velocity of the boundary is periodic, with the former exhibiting convex-upward segments and the latter concave-upward segments, in each case separated by rapid changes in velocity [transitions]. Both convex-upward [22,28] and concave-upward kinetics [33] are observed in experimental systems.

Periodic boundary motion leaves behind a spatially periodic pattern whose wavelength is determined by the mean velocity and the frequency of transitions. If this wavelength is one for which stable Turing patterns can exist in an infinite domain, the pattern will generally persist, but in other cases it may evolve through peak decay or peak splitting to a different [and stable] wavelength, or it may decay to a homogeneous state.

### ACKNOWLEDGMENTS

This research was supported by the Consortium for Advanced Simulation of Light Water Reactors, an Energy Innovation Hub for Modeling and Simulation of Nuclear Reactors under U.S. Department of Energy Contract No. DE-AC05-00OR22725.

### APPENDIX A: GIERER-MEINHARDT MODEL: DIMENSIONLESS FORMULATION

Gierer and Meinhardt [10] defined their activator-inhibitor model through the equations

$$\frac{\partial u}{\partial t} = D_u \frac{\partial^2 u}{\partial x^2} + c_1 v^2 - c_2 u, \quad \frac{\partial v}{\partial t} = D_v \frac{\partial^2 v}{\partial x^2} + \frac{c_3 v^2}{u} - c_4 v. \quad (A1)$$

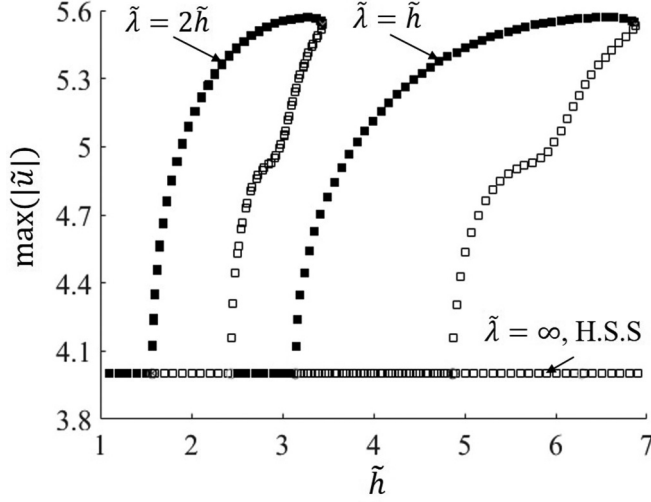


FIG. 6. Bifurcation diagram for Gierer-Meinhardt activator ( $v$ )-inhibitor ( $u$ ) kinetics with  $R_D = 3/40$ ,  $\tilde{c}_3 = 1.0$ ,  $\tilde{c}_4 = 0.5$  (case [B] in Fig. 3), assuming the domain to be fixed. Solid squares represent the stable steady states while hollow squares mark the unstable steady-states, obtained under zero-flux boundary conditions. Stable patterns are obtained in the wavelength range of  $3.1 < \tilde{\lambda} < 6.8$  (bounds  $\tilde{\lambda}_1^B, \tilde{\lambda}_2^B$ ). H.S.S stands for the homogeneous-steady-state solution of Eq. (6).

For the moving boundary problem we use the boundary conditions and growth law

$$\begin{aligned} u(0, t) = u_0, \quad \frac{\partial v}{\partial x}(0, t) = 0, \quad v(h, t) = v_h, \\ -D_u \frac{\partial u}{\partial x}(h, t) = [u(h, t) + Q] \frac{dh}{dt}, \quad \frac{dh}{dt} = ku(h, t). \end{aligned} \quad (\text{A2})$$

A dimensionless form of these equations can be obtained by defining

$$\begin{aligned} \tilde{u} = \frac{c_1 u}{c_2}, \quad \tilde{v} = \frac{c_1 v}{c_2}, \quad \tilde{x} = x \sqrt{\frac{c_2}{D_u}}, \\ \tilde{t} = c_2 t, \quad \tilde{h} = h \sqrt{\frac{c_2}{D_u}}. \end{aligned} \quad (\text{A3})$$

Using these expressions in the governing Eqs. (A1) and the boundary conditions (A2) we obtain Eqs. (5) and (8) to (10), respectively, where

$$\begin{aligned} R_D = \frac{D_v}{D_u}, \quad \tilde{c}_3 = \frac{c_3}{c_2}, \quad \tilde{c}_4 = \frac{c_4}{c_2}, \quad \tilde{u}_0 = \frac{c_1 u_0}{c_2}, \\ \tilde{v}_h = \frac{c_1 v_h}{c_2}, \quad \tilde{Q} = \frac{c_1 Q}{c_2}, \quad \tilde{k} = \frac{k}{c_1} \sqrt{\frac{c_2}{D_u}} \end{aligned} \quad (\text{A4})$$

are the independent dimensionless parameters defining the system.

Nesterenko *et al.* [34] derived the condition

$$\frac{D_u}{D_v} > \frac{c_2}{(3 - 2\sqrt{2})c_4} \quad (\text{A5})$$

for the homogeneous solution of Eq. (A1) to be unstable, leading to the formation of Turing patterns. Using the notation of Eq. (A4), this can be expressed in the form of Eq. (7).

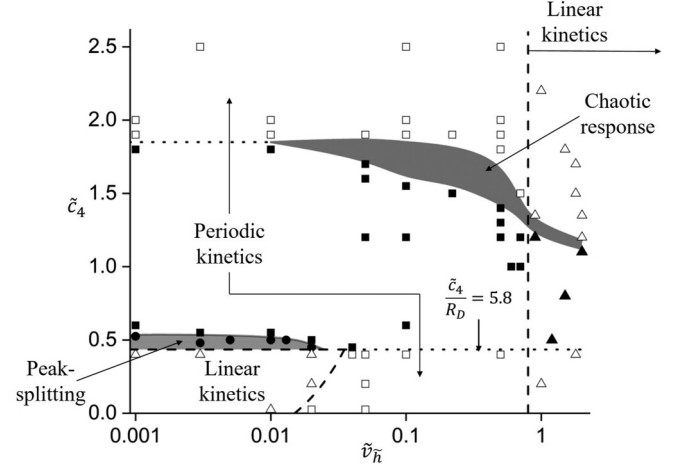


FIG. 7. The solid symbols in this map indicate numerical simulations that resulted in pattern formation, and the open symbols indicate numerical simulations that did not result in pattern formation. The triangular symbols indicate conditions under which the boundary moved in a linear fashion, rather than in a periodic fashion. The lower shaded area, and the corresponding circular points, represent a region in which peak-splitting was observed. The upper shaded region represents where chaotic, random behavior was observed that was very sensitive with respect to small changes in the values of input parameters. The lower dotted line corresponds to the condition  $\tilde{c}_4 = 5.8R_D$ , which is the instability condition of Eq. (7). These results were obtained using Gierer-Meinhardt activator ( $v$ )-inhibitor ( $u$ ) kinetics with  $R_D = 0.075$ ,  $\tilde{c}_3 = 1$ ,  $\tilde{u}_0 = 1$ ,  $\tilde{Q} = 1$ , and  $\tilde{k} = 1$ .

## APPENDIX B: STATIONARY SOLUTIONS OF THE GIERER-MEINHARDT MODEL IN FIXED DOMAINS

In this Appendix, we discuss the numerical procedure for determining stable and unstable steady states of the Gierer-Meinhardt model of Eq. (5) in a fixed domain. We achieve this using MATLAB's continuation and bifurcation package PDE2PATH [31,32].

We use  $\tilde{h}$  as the bifurcation parameter for analyzing the PDEs in Eqs. (11) and (12), while neglecting the advection terms containing  $d\tilde{h}/d\tilde{t}$  (i.e., in a fixed domain  $0 < \zeta < 1$  where  $\zeta = \tilde{x}/\tilde{h}$ ). Zero-flux boundary conditions are used. For the purpose of demonstration, we show results for parameters of case [B] of Sec. IIC ( $R_D = 3/40$ ,  $\tilde{c}_3 = 1.0$ ,  $\tilde{c}_4 = 0.5$ ) in Fig. 6. The trajectory of concentration of species  $\tilde{u}$  is represented by its maximum absolute value,  $\max(|\tilde{u}|)$ . The solid and hollow squares represent stable and unstable solutions, respectively. The horizontal branch at  $\max(|\tilde{u}|) = 4$  corresponds to the homogeneous steady state of Eq. (6). The other two branches,  $\tilde{\lambda} = 2\tilde{h}$  and  $\tilde{\lambda} = \tilde{h}$ , correspond to stationary periodic solutions, found to be stable in the range  $3.1 < \tilde{\lambda} < 6.8$ . Notice that the boundary conditions support solutions with an integer number of half-waves in the domain. Note that for this case, the homogeneous-steady-state is unstable to small perturbations with wavelengths in a significantly smaller range of  $3.1 < \tilde{\lambda} < 4.8$ . This shows that a linear stability analysis about the homogeneous solution gives only an imperfect guide to the range of wavelengths to be expected in a transient simulation.

For case [A] of Sec. II C, stable patterns in the range  $2.6 < \tilde{\lambda} < 21$  were obtained using a similar procedure. Note that PDE2PATH permits fairly general dependence of the coefficients on  $\tilde{u}$ ,  $\tilde{v}$ , and  $\zeta$  but not on time  $\tilde{t}$ , so it cannot be applied to the moving-boundary problem of Eqs. (11) and (12), even if the domain growth  $\tilde{h}(\tilde{t})$  were specified or approximated.

**APPENDIX C: BEHAVIORAL MAP OF THE ACTIVATOR-INHIBITOR MODEL**

Shifts in the response of the activator-inhibitor model of Sec. II, with respect to the change in the dimensionless parameters  $\tilde{v}_{\tilde{h}}$  and  $\tilde{c}_4$ , are shown in Fig. 7. While nonlinear boundary kinetics of convex-up segments [as shown in Fig. 1(a)] are observed for lower values of the activator concentration  $\tilde{v}_{\tilde{h}}$ , increasing it beyond  $\sim 1$  results in a local buildup of the inhibitor concentration ( $\tilde{u}$ ) at the moving front, which then moves linearly in response. For regions not satisfying the instability condition of Eq. (7), i.e., for  $\tilde{c}_4 < 5.8R_D$ , no patterns are observed. However, boundary kinetics still shows a periodicity for some of such cases. As we move away from this region by increasing  $\tilde{c}_4$ , a general trend of pattern formation, chaotic concentration distribution, followed by no pattern formation, is observed. Notice that as the solution is numerical, this map does not provide any general conclusions for all parameter ranges, as opposed to a linear stability analysis [35–37]. However, as shown in Appendix B, a linear stability analysis only provides a subset of wavelengths which form stable patterns in reaction-diffusion systems of Eqs. (5) and (17).

**APPENDIX D: SCHNAKENBERG MODEL: DIMENSIONLESS FORMULATIONS**

The governing differential equations for the Schnakenberg model [11] are

$$\begin{aligned} \frac{\partial u}{\partial t} &= D_u \frac{\partial^2 u}{\partial x^2} - c_1 v^2 u + a, \\ \frac{\partial v}{\partial t} &= D_v \frac{\partial^2 v}{\partial x^2} + c_1 v^2 u - c_2 v + b. \end{aligned} \tag{D1}$$

We use the same boundary conditions and growth law (A2) as in the Geirer-Meinhardt model. A dimensionless formulation can then be obtained by defining

$$\tilde{u} = \mu u, \quad \tilde{v} = \mu v, \quad \tilde{x} = x \sqrt{\frac{c_2}{D_u}}, \quad \tilde{h} = h \sqrt{\frac{c_2}{D_u}}, \quad \tilde{t} = c_2 t \tag{D2}$$

[16], where  $\mu = \sqrt{c_1/c_2}$ . Substituting these relations in Eq. (D1), we obtain the dimensionless governing Eqs. (17). The corresponding dimensionless boundary conditions and growth law are unchanged from Eqs. (8) to (10). In this case, the independent dimensionless parameters defining the system comprise

$$\begin{aligned} R_D &= \frac{D_v}{D_u}, \quad \tilde{a} = \frac{\mu a}{c_2}, \quad \tilde{b} = \frac{\mu b}{c_2}, \quad \tilde{u}_0 = \mu u_0, \\ \tilde{v}_h &= \mu v_h, \quad \tilde{Q} = \mu Q, \quad \tilde{k} = \frac{k}{\sqrt{D_u c_1}}. \end{aligned} \tag{D3}$$

---

[1] A. M. Turing, The Chemical Basis of Morphogenesis, *Philos. Trans. R. Soc. London B* **237**, 37 (1952).

[2] J. D. Murray, How the leopard gets its spots, *Sci. Am.* **258**, 80 (1988).

[3] S. Kondo and R. Asai, A reaction–diffusion wave on the skin of the marine angelfish pomacanthus, *Nature* **376**, 765 (1995).

[4] H. Meinhardt and M. Klingler, A model for pattern formation on the shells of molluscs, *J. Theor. Biol.* **126**, 63 (1987).

[5] R. L. Cooper, A. P. Thiery, A. G. Fletcher, D. J. Delbarre, L. J. Rasch, and G. J. Fraser, An ancient turing-like patterning mechanism regulates skin denticle development in sharks, *Sci. Adv.* **4**, eaau5484 (2018).

[6] A. D. Economou, A. Ohazama, T. Pomtaveetus, P. T. Sharpe, S. Kondo, M. A. Basson, A. Gritli-Linde, M. T. Cobourne, and J. B. Green, Periodic stripe formation by a turing mechanism operating at growth zones in the mammalian palate, *Nat. Genet.* **44**, 348 (2012).

[7] M. A. Chaplain, M. Ganesh, and I. G. Graham, Spatio-temporal pattern formation on spherical surfaces: Numerical simulation and application to solid tumour growth, *J. Math. Biol.* **42**, 387 (2001).

[8] C. A. Klausmeier, Regular and irregular patterns in semiarid vegetation, *Science* **284**, 1826 (1999).

[9] M. Mimura and J. Murray, On a diffusive prey-predator model which exhibits patchiness, *J. Theor. Biol.* **75**, 249 (1978).

[10] A. Gierer and H. Meinhardt, A theory of biological pattern formation, *Kybernetik* **12**, 30 (1972).

[11] J. Schnakenberg, Simple chemical reaction systems with limit cycle behaviour, *J. Theor. Biol.* **81**, 389 (1979).

[12] I. Prigogine and R. Lefever, Symmetry breaking instabilities in dissipative systems. ii, *J. Chem. Phys.* **48**, 1695 (1968).

[13] A. Nakamasu, G. Takahashi, A. Kanbe, and S. Kondo, Interactions between zebrafish pigment cells responsible for the generation of turing patterns, *Proc. Natl. Acad. Sci. USA* **106**, 8429 (2009).

[14] E. J. Crampin, E. A. Gaffney, and P. K. Maini, Reaction and diffusion on growing domains: Scenarios for robust pattern formation, *Bull. Math. Biol.* **61**, 1093 (1999).

[15] E. Crampin and P. Maini, Reaction-diffusion models for biological pattern formation, *Meth. Appl. Anal.* **8**, 415 (2001).

[16] E. Crampin, W. Hackborn, and P. Maini, Pattern formation in reaction-diffusion models with nonuniform domain growth, *Bull. Math. Biol.* **64**, 747 (2002).

[17] A. Madzvamuse, Time-stepping schemes for moving grid finite elements applied to reaction–diffusion systems on fixed and growing domains, *J. Comput. Phys.* **214**, 239 (2006).

[18] A. Neville, P. Matthews, and H. Byrne, Interactions between pattern formation and domain growth, *Bull. Math. Biol.* **68**, 1975 (2006).

[19] S. S. Lee, E. Gaffney, and R. Baker, The dynamics of turing patterns for morphogen-regulated growing domains with cellular response delays, *Bull. Math. Biol.* **73**, 2527 (2011).



- [20] A. L. Krause, M. A. Ellis, and R. A. Van Gorder, Influence of curvature, growth, and anisotropy on the evolution of turing patterns on growing manifolds, *Bull. Math. Biol.* **81**, 759 (2019).
- [21] I. Heath, *Tip Growth in Plant and Fungal Cells* (Elsevier Science, New York, 2013).
- [22] A. T. Motta, A. Couet, and R. J. Comstock, Corrosion of zirconium alloys used for nuclear fuel cladding, *Annu. Rev. Mater. Res.* **45**, 311 (2015).
- [23] G. Gu and H. Peng, Numerical simulation of reaction-diffusion systems of turing pattern formation, *Internat. J. Mod. Nonl. Theory Appli.* **4**, 215 (2015).
- [24] P. N. McGraw, M. Menzinger, and A. P. Muñozuri, Harmonic resonant excitation of flow-distributed oscillation waves and turing patterns driven at a growing boundary, *Phys. Rev. E* **80**, 026209 (2009).
- [25] M. Kærn, M. Menzinger, and A. Hunding, Segmentation and somitogenesis derived from phase dynamics in growing oscillatory media, *J. Theor. Biol.* **207**, 473 (2000).
- [26] M. Kærn, M. Menzinger, R. Satnoianu, and A. Hunding, Chemical waves in open flows of active media: Their relevance to axial segmentation in biology, *Faraday Discuss.* **120**, 295 (2002).
- [27] A. Krichevsky, S. V. Kozlovsky, G.-W. Tian, M.-H. Chen, A. Zaltsman, and V. Citovsky, How pollen tubes grow, *Dev. Biol.* **303**, 405 (2007).
- [28] E. Pierson, Y. Li, H. Zhang, M. Willemse, H. Linskens, and M. Cresti, Pulsatory growth of pollen tubes: Investigation of a possible relationship with the periodic distribution of cell wall components, *Acta Bot. Neerl.* **44**, 121 (1995).
- [29] M. Stępką, F. Ciampolini, M. Charzyńska, and M. Cresti, Localization of pectins in the pollen tube wall of *Ornithogalum virens* L. Does the pattern of pectin distribution depend on the growth rate of the pollen tube?, *Planta* **210**, 630 (2000).
- [30] B. E. Deal and A. Grove, General relationship for the thermal oxidation of silicon, *J. Appl. Phys.* **36**, 3770 (1965).
- [31] I. Barrass, E. J. Crampin, and P. K. Maini, Mode transitions in a model reaction-diffusion system driven by domain growth and noise, *Bull. Math. Biol.* **68**, 981 (2006).
- [32] PDE2PATH - a MATLAB package for continuation and bifurcation in systems of PDEs, v2.8, <http://www.staff.uni-oldenburg.de/hannes.uecker/pde2path/>.
- [33] S. Y. Kondratev, G. P. Anastasiadi, A. V. Ptashnik, and S. N. Petrov, Kinetics of the high-temperature oxidation of heat-resistant statically and centrifugally cast HP<sub>40</sub>NbTi alloys, *Oxid. Met.* **91**, 33 (2019).
- [34] A. M. Nesterenko, M. B. Kuznetsov, D. D. Korotkova, and A. G. Zharisky, Morphogene adsorption as a turing instability regulator: Theoretical analysis and possible applications in multicellular embryonic systems, *PLoS One* **12**, e0171212 (2017).
- [35] A. Madzvamuse, Stability analysis of reaction-diffusion systems with constant coefficients on growing domains, *Intern. J. Dyn. Syst. Diff. Eqs.* **1**, 250 (2008).
- [36] A. Madzvamuse, E. A. Gaffney, and P. K. Maini, Stability analysis of non-autonomous reaction-diffusion systems: The effects of growing domains, *J. Math. Biol.* **61**, 133 (2010).
- [37] R. A. Van Gorder, V. Klika, and A. L. Krause, Turing conditions for pattern forming systems on evolving manifolds, [arXiv:1904.09683v2](https://arxiv.org/abs/1904.09683v2).